Design and analysis of differential passive circuits for I/Q generation in 60 GHz integrated circuits

Ivan M. Milosavljević [1, 2], Dušan P. Krčum [1, 2], Lazar V. Saranovac [1]

[1]Department of Electronics, School of Electrical Engineering, University of Belgrade, Bulevar kralja Aleksandra 73, Belgrade, Serbia

[2] NovelIC, Omladinskih brigada 86p, Belgrade, Serbia

Abstract: I/Q generation circuit design is of great importance within the design of modern radars integrated on chip, as well as in high-speed communication circuits operating at millimeter wave frequencies. Due to increased robustness on process variations and noise, differential signaling and differential I/Q generators are of particular interest. Several passive topologies suitable for usage in the commercially available 130 nm SiGe BiCMOS process are presented and evaluated. These topologies are: branch-line coupler (BLC), broadside coupler (BSC), poly-phase filter (PPF) and quadrature all-pass filter (QAF). The first three topologies are implemented and the obtained results are compared to results published previously. The designed PPF has a total phase error of $\pm 2.5°$ over a 40 GHz bandwidth and this is the most desired solution if the total available area is a limiting factor. Transmission lines required for the design of BLC and BSC are small enough, making such structures easy to implement using today's mainstream technologies. BLC is a reliable and widely used solution for I/Q generation at almost any microwave frequency. Designed BLC has a phase error of $\pm 1.7°$ over a 7 GHz bandwidth. BSC has proved to be the best solution for I/Q generation in the 60 GHz band. The designed solution has a smaller area than BLC, a phase error of only $\pm 5°$ over a 40 GHz bandwidth and $\pm 1°$ over a 7 GHz bandwidth.

Keywords: millimeter-wave passive circuits, I/Q generation, 90° hybrid coupler, branch-line coupler, broadside coupler, poly-phase filter, quadrature all-pass filter

* Corresponding Author's email: ivan.milosavljevic@novelic.com

Introduction

Today's millimeter-wave integrated circuits are primarily intended for communication and radar sensing applications. Advancements in silicon-based technology processes allowed the very high scale integration, making complete millimeter-wave systems integrated into a single chip. In these complex systems, usually there is a need for the generation of in-phase (I) and quadrature (Q) signals [1-5]. As an example, for blocks such as I/Q modulators [6], frequency multipliers [7], or vector-modulators [8-10], it is mandatory to have supporting circuits that provide the desired 90° phase shift between the input signals, in cases when quadrature signals are not provided by the local oscillator (LO). Direct I/Q signal generation from the LO requires the design of a quadrature voltage controlled oscillator (QVCO). Although the design of a conventional parallel-coupled QVCO at millimeter-wave frequencies is feasible and reported in [11], the approach suffers from very high phase noise, and therefore its usage is limited. There are other QVCO state-of-the-art techniques based on injection- [12] and magnetic-coupling [13] that improve phase-noise, but their complexity and reliability issues rise with frequency. At microwave frequencies 90° phase generation can be provided by active quadrature dividers [14]. The use of dividers requires the VCO operating at twice the nominal frequency, therefore at higher millimeter-wave frequencies this is not a suitable topology. Another approach is using injection-locked frequency multipliers [15], that also suffer from similar problems as the approach with QVCO. Furthermore, using active circuits for I/Q generation requires current-hungry and more sophisticated designs at millimeter-wave frequencies. In opposite to active circuits, passive circuits do not consume power. However, they introduce some losses that often need to be compensated, and the total loss per branch cannot be smaller than the theoretical minimum of 3 dB. Besides consumption, the key advantages of passive circuits are design simplicity and reliability. Consequently, a natural choice for I/Q signal generation at millimeter-wave frequencies is a passive circuit.

There are various ways of generating quadrature signals with passive circuits based on quarter-wave ($\lambda/4$) coupled and transmission line millimeter-wave structures. The limiting factor for quarter-wave structures, also known in literature as 90° hybrid couplers, is chip area which is directly related to signal wavelength. This is the reason why these structures are much more interesting nowadays when the majority of high-speed communication systems operating frequencies are shifted to the millimeter-wave area. Passive quarter-wave structures for microwave frequencies have been investigated at various substrates. The investigations are mainly focused on miniaturization of quarter-wave coupled structures, as reported in [16, 17]. Most of them only deal with single-ended circuits, not suitable for integration in high-performance integrated circuits. Therefore this paper is focused only on topologies that have differential counterparts, in order to minimize sensitivity to noise and undesired couplings. On the other hand, passive circuits for quadrature generation are also designed from lumped components. The main representatives are RC and RLC based circuits and a

vast number of papers comprised of circuits at millimeter-wave frequencies have been reported [18-20].

The article is organized as follows: section 2 shows theoretical basics of different passive circuits for I/Q generation. Implementation of circuits and simulation results obtained with electromagnetic (EM) solvers are shown in Section 3, followed by conclusions in Section 4.

2 Passive circuits for I/Q generation

The main parameters of passive circuits for I/Q generation are reflection coefficients, insertion loss, coupling, directivity, bandwidth, phase imbalance, amplitude imbalance, isolation between output ports and chip area. The priority of parameters is determined by specific application. Typically in millimeter-wave integrated circuits, the highest priority parameters are phase imbalance, insertion loss and chip area.

Based on physical phenomena of quadrature generation, passive circuits are divided in two main categories: I/Q generators based on distributed structures (transmission lines) and I/Q generators based on lumped components.

2.1 Distributed

Transmission line-based passive circuits provide 90° phase shift using quarter-wave segments of transmission lines. The most basic representative is the one with $\lambda/4$ transmission line inserted in the quadrature signal path. This approach requires a power divider for splitting the input signal in two signals of equal power. If a Wilkinson power divider [21] is used, significant chip area is required. In Figure 1, differential structures based on 90° transmission lines are shown. The input differential signal is LO, and the outputs are differential in-phase (I) and quadrature (Q) signals. Conventional approach shown in Figure 1 (a) suffers from narrowband operation, which can be improved using the Schiffman technique shown in Figure 1 (b) [22]. With this technique, performance is improved at the expense of chip area. Both implementations are impractical in millimeter-wave integrated circuits due to increased area and attenuation.

Alternatively, distributed structures based on concentrated coupling and coupled transmission lines are widely used in millimeter-wave integrated circuits.

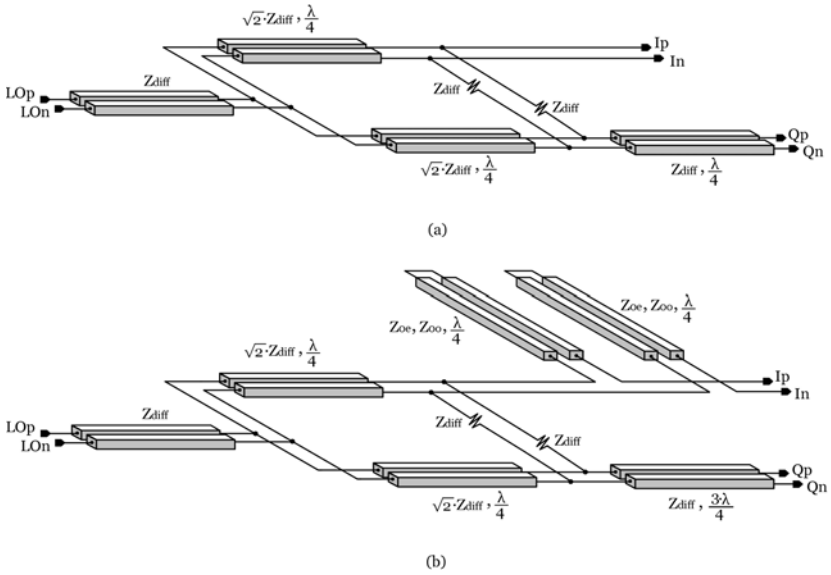

Figure 1: (a) 90° transmission line based power divider, (b) Schiffman 90°power divider.

2.1.1 Concentrated coupling

Branch-line coupler (BLC) is a representative of transmission lines concentrated coupling. Conventional BLC hybrid is shown in Figure 2 (a). Since it occupies considerable chip area, reduction of transmission lines length is proposed in [16], by inserting shunt capacitance at the end of the transmission lines. This is shown in Figure 2 (b).

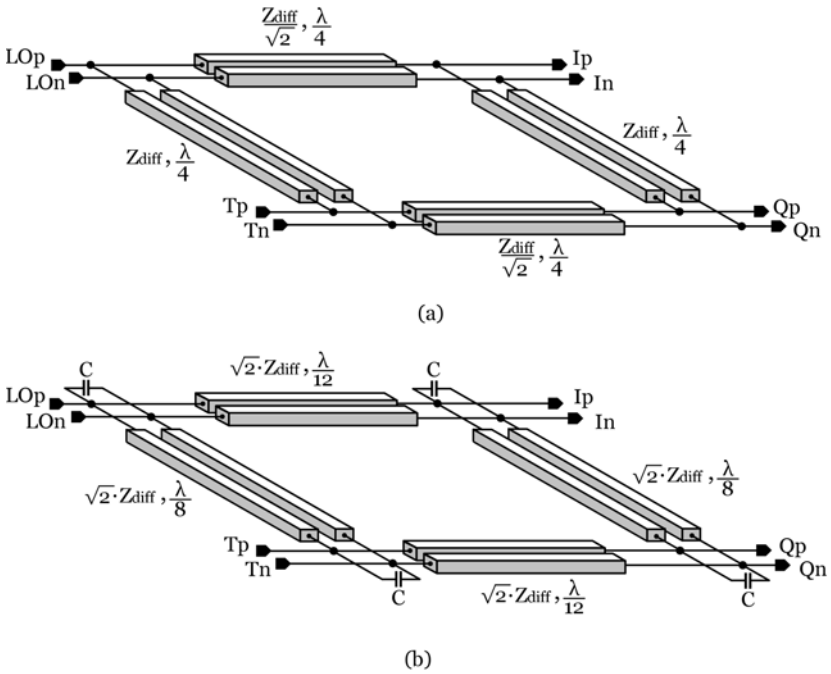

Figure 2: (a) Conventional branch-line coupler, (b) Reduced size branch-line coupler.

The relationships between electrical lengths of branch-line θ_1 and through-line θ_2, the differential characteristic impedance Z, the nominal differential impedance Z_{diff}, and shunt capacitance C in reduced-size BLC hybrid are given as

$$\theta_1 = arcsin\left(\frac{Z_{diff}}{Z}\right), \tag{1}$$

$$\theta_2 = arcsin\left(\frac{Z_{diff}}{\sqrt{2}Z}\right), \tag{2}$$

$$\omega C Z_{diff} = \sqrt{1-\left(\frac{Z_{diff}}{Z}\right)^2} + \sqrt{2-\left(\frac{Z_{diff}}{Z}\right)^2} \tag{3}$$

In Figure 2 (b) it is given commonly used case when $Z_{diff}/Z = 1/\sqrt{2}$, $\theta_1 = 30°$ and $\theta_2 = 45°$. These values are very suited for practical implementations. Additionally, a technique of meandering is implemented whenever applicable to reduce total chip area.

2.1.2 Coupled line

In microwave theory, I/Q generators based on coupled lines are known as directional couplers. Directional couplers are easily constructed from two $\lambda/4$ coupled transmission lines. The coupling effect is achieved by broadside coupling or edge-side coupling, as shown in Figure 3. The coupling ratio between two broadside coupled metal layers is given by

$$k = \frac{Z_{0e} - Z_{0o}}{Z_{0e} + Z_{0o}} = \sqrt{\epsilon_r} \times k_{air}, \tag{4}$$

where Z_{0e} and Z_{0o} are even- and odd-mode impedances of the coupled lines, ϵ_r is the relative permittivity of the substrate, and k_{air} is the coupling factor of the two lines in air.

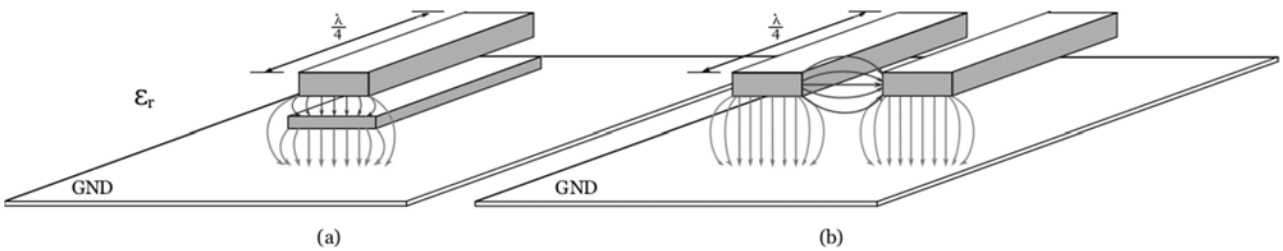

Figure 3: (a) Broadside coupling, (b) Edge-side coupling

In integrated realizations, the broadside coupler (BSC) is suitable for implementation, and its vertical approach saves chip area. An important issue is that the distributed capacitance from the broadside coupled lines to the ground is asymmetric. Therefore, the width of transmission lines must be asymmetric to minimize asymmetry and optimize bandwidth, as shown in Figure 3 (a).

Alternatively, edge-side coupled structures shown in Figure 3 (b) can be used. They are very simple to design, but suffer from several issues. Due to its inhomogeneous dielectric nature, modal velocities of even- and odd-modes are different. This difference leads to poor isolation and, consequently, worse directivity of the coupler. In order to overcome this problem, modal velocities should be equalized. Within practical solutions for equalization, the most suitable one for integrated circuit (IC) design is the placement of capacitors between input and output ports. However, even after applying this technique, overall performance of edge-side coupler remains mediocre. The edge-side coupler also suffers from reliability issues due to fabrication and tolerance problems.

As a solution, multiple transmission lines are interdigitated in edge-side couplers. This structure is known as a Lange coupler [23], and the key design parameter is the voltage coupling coefficient c. Improved coupling helps in relaxing fabrication and tolerance problems. Millimeter-wave designs of single-ended unfolded Lange coupler are reported in [8, 24], etc. Differential Lange coupler requires two single-ended Lange structures that significantly increase the area and complexity of the circuit, therefore they are rarely used.

2.2 Lumped components based

Passive circuits for quadrature signal generation can be realized using basic circuit elements such as resistors, capacitors and inductors. Mentioned elements can easily be implemented in currently available silicon-based processes. This approach in generation of quadrature signals leads to simple, inexpensive and very compact design. However, this design has large losses and a significant central frequency shift which is temperature and process dependent. Circuits for I/Q generation that use lumped elements are unable to handle larger power levels. In practical designs, two main circuit topologies are used: poly-phase filter (PPF) and quadrature all-pass filter (QAF).

2.2.1 Poly-phase filters

PPF quadrature generation is based on phase shaping using combination of low-pass and high-pass RC filters. Low-pass (LPF) and high-pass filter (HPF) transfer functions are given by

$$H_{LPF}(j\omega) = \frac{1}{1 + j\omega RC}, \tag{5}$$

$$H_{HPF}(j\omega) = \frac{j\omega RC}{1 + j\omega RC}. \tag{6}$$

Corresponding arguments are:

$$\theta_{LPF} = -arctg(\omega RC), \tag{7}$$

$$\theta_{HPF} = \frac{\pi}{2} - arctg(\omega RC). \tag{8}$$

If the values of the components in LPF and HPF are chosen as $RC = \frac{1}{\omega_0}$, where ω_0 is radial frequency of an input signal, phase shift through a LPF is $-45°$ and through HPF is $+45°$, while attenuation is equal in both paths.

The first order PPF achieves a narrowband quadrature generation and has a wide phase variation over process and temperature. More robust design can be obtained using higher order PPF. Second order PPFs are widely used, as shown in Figure 4. In order to reduce influence of the process variations, component values of each PPF stage are chosen for a different central frequency:

$$R_1 C_1 = \frac{1}{\omega_1}, \tag{9}$$

$$R_2 C_2 = \frac{1}{\omega_2}. \tag{10}$$

Relationship between the input radial frequency and poles of PPF is given by

$$\omega_1 \omega_2 = \omega_0^2, \tag{11}$$

where $\omega_1 < \omega_0 < \omega_2$.

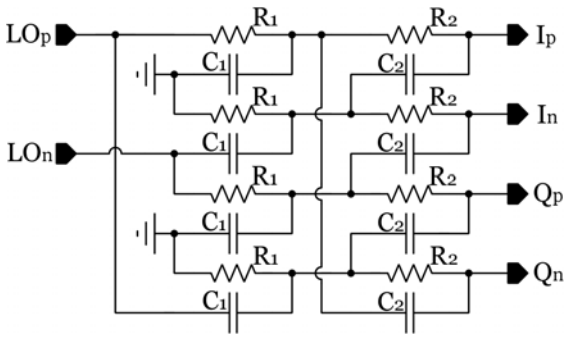

Figure 4: Second order PPF schematic.

2.2.2 Quadrature all-pass filter

QAF is used for phase shaping of quadrature output signals. In Figure 5, is shown the schematic of a fully differential QAF.

Theory of operation is similar to PPF. Namely, QAF also uses combination of LPF and HPF for adequate phase shift between the output signals. Transfer functions between LO input and I and Q outputs are given in equations (12) and (13):

$$H_I(j\omega) = \frac{R + j\omega L}{R + j\left(\omega L - \frac{1}{\omega C}\right)}, \tag{12}$$

$$H_Q(j\omega) = \frac{R + \frac{1}{j\omega C}}{R + j\left(\omega L - \frac{1}{\omega C}\right)}. \tag{13}$$

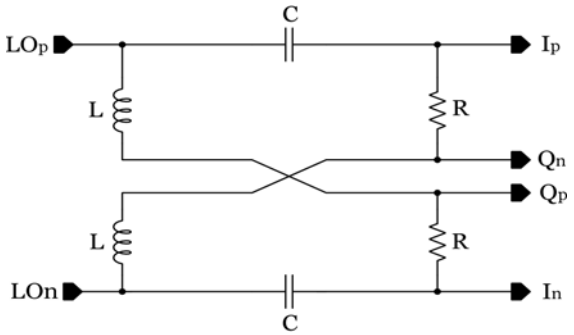

Figure 5: LC based QAF schematic

Phase difference between QAF outputs can be derived from the previous transfer functions, and after simplification the final expression for the QAF phase difference is:

$$\theta_{QAF} = arctg\left(\frac{\omega^2 LC + 1}{\omega\left(RC - \frac{L}{R}\right)}\right). \tag{14}$$

In order to make the phase difference between I and Q signals equal to 90^0, the resistance value should be

$$R = \sqrt{\frac{L}{C}}, \tag{15}$$

and for equal attenuation in both paths

$$LC = \left(\frac{1}{\omega_0}\right)^2. \tag{16}$$

3 Implementation and simulation results

In this section, different passive I/Q generators are implemented using a commercially available 130 nm SiGe BiCMOS technology with seven metal layers shown in Figure 6.

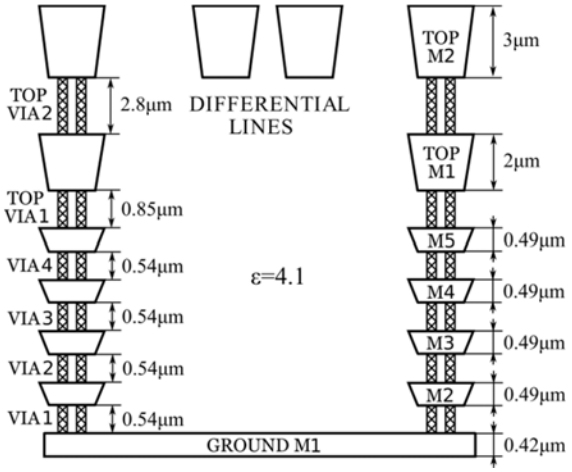

Figure 6: Technology metal stack.

In all implementations solid metal 1 is used as circuit ground. All passive circuits are simulated in 2.5D planar EM solver based on method of moments (MoM), and verified in 3D full-wave solver based on finite element method (FEM). The comparison between simulation results is given for all designed circuits. The results obtained with MoM based simulator are shown as dashed lines, and the results obtained with FEM based simulator as solid lines. Impact of the mismatch and process variations of resistors and capacitors on phase and amplitude imbalance is simulated for all circuits using Monte Carlo simulations. Influence of the output load mismatch is also analyzed. Output impedances of both I and Q loads are varied in range 80% - 120% of nominal 100 Ω differential impedance. Effect of the mismatch and process variations and load mismatch is analyzed on single frequency of 60 GHz and characterized using $\pm 3\sigma$ (standard deviation).

3.1 Branch-line coupler

Implementation of differential reduced-size BLC is presented in this subsection. Transmission lines are implemented in 3 μm thick top metal 2. Differential impedance of branch-line and through-line is 141.4 Ω, which corresponds to lines of width 3 μm and spacing 17 μm. Transformation to a differential impedance of 100 Ω at input and output ports is achieved by reducing line spacing to 7 μm and retaining same widths. According to equation (3), 43 fF differential capacitor value is obtained. Metal-insulator-metal (MIM) capacitors are used. In this technology, the bottom electrode of the MIM capacitor is connected to metal 5 and the top electrode to top metal 1. Thus, two serial capacitors with twice the capacitance are used instead of a single differential capacitor. Capacitors are made in such a way to fit between differential lines and are connected in metal 5. 3D preview of the

reduced-size BLC is shown in Figure 7. A meandering technique is used to reduce the overall BLC area, which is 267 μm x 230 μm.

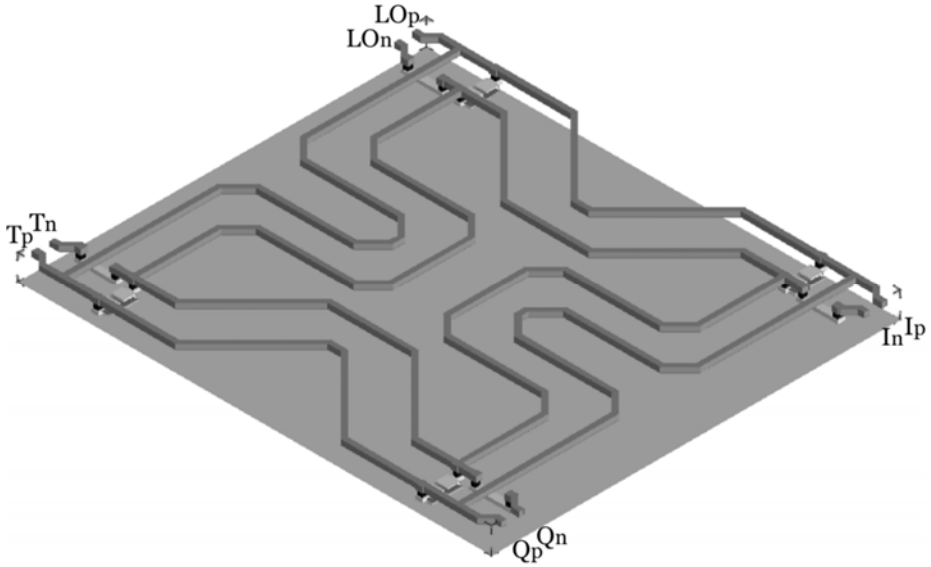

Figure 7: 3D preview of the differential branch-line coupler.

The termination port is connected to a 100 Ω resistor and the performance of the 60 GHz BLC obtained by MoM and FEM based simulators are shown in Figure 8.

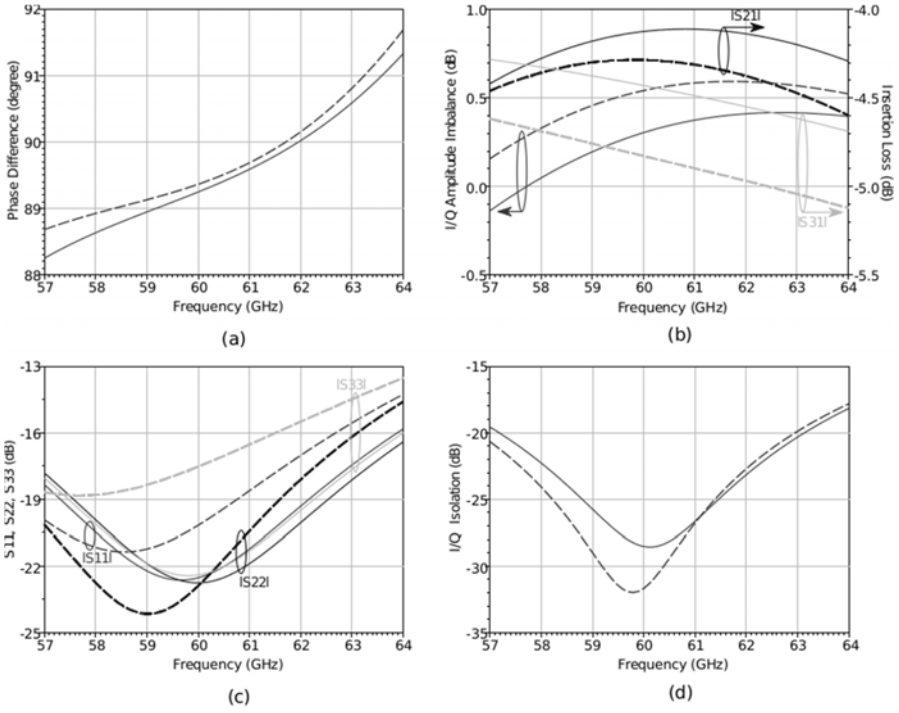

Figure 8: The performance of differential branch-line coupler: (a) phase difference, (b) insertion loss, (c) reflection coefficient, (d) isolation.

The BLC exhibits excellent performance in a 7 GHz bandwidth. Phase imbalance of the BLC is lower than 1.7°, and amplitude imbalance is lower than 0.4 dB. Reflection coefficients at input and outputs are lower than -14 dB. Performing process and mismatch Monte Carlo simulations gave us the insight in circuit's behavior under mentioned conditions. It is noticed that phase and amplitude imbalance does not vary more than 2.42º and 0.14 dB in the case of process and mismatch variations of the termination resistor and MIM capacitors. Major contributor on phase and amplitude imbalance deviation is the process variation of MIM capacitors and this should be taken into account in design process of reduced-size BLC. I/Q load mismatch effect on the phase imbalance is lower than 0.76º, while the amplitude imbalance is negligible.

3.2 Broadside coupler

Differential input and output signals of the BSC are implemented in top metal 2 layer. Transmission lines are optimized to a differential impedance of 100 Ω. The width of lines is 3.5 μm and spacing is 4.5 μm. Coupled $\lambda/4$ lines are implemented in top metal 1 and metal 5 to achieve high coupling efficiency. Inter-layer distance is 0.85 μm. It requires the coupling coefficient k of $1/\sqrt{2}$, and according to equation (4) values for even- and odd-mode impedances are approximately 241.5 Ω and 41.4 Ω. The widths of coupled lines are calculated from the EM simulation and top metal width of 5 μm and bottom metal width of 8 μm are obtained. In Figure 9, the geometry of 60 GHz differential BSC is shown. Aggressive meandering of the coupled lines is performed to minimize chip area. The BSC dimensions are 190 μm x 170 μm.

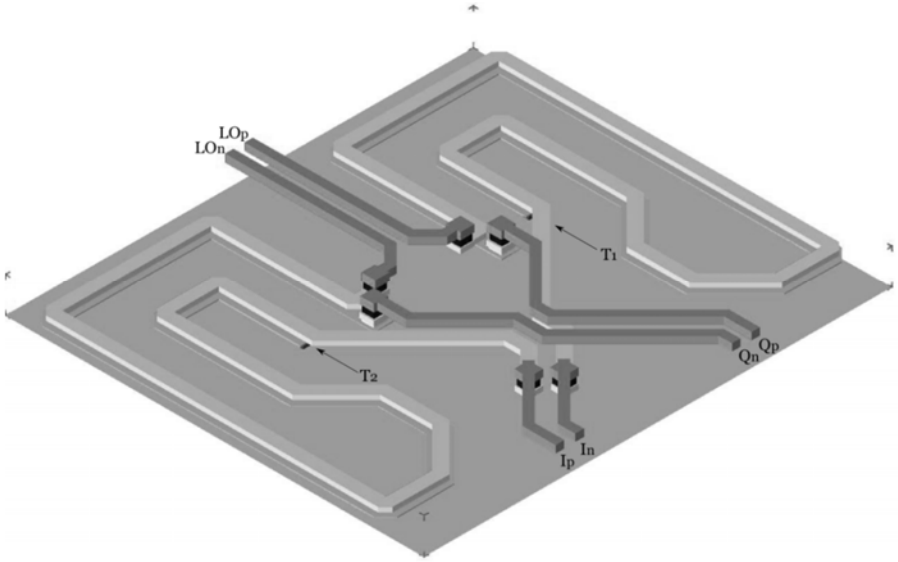

Figure 9: 3D preview of the differential broadside coupler.

Termination impedances T1 and T2 are chosen to be asymmetric in order to achieve very low phase mismatch. In this way the amplitude difference is consciously sacrificed. Termination

impedance T1 is 20 Ω, and termination impedance T2 is 50 Ω. The performance of the 60 GHz BSC obtained by MoM and FEM simulators are shown in Figure 10.

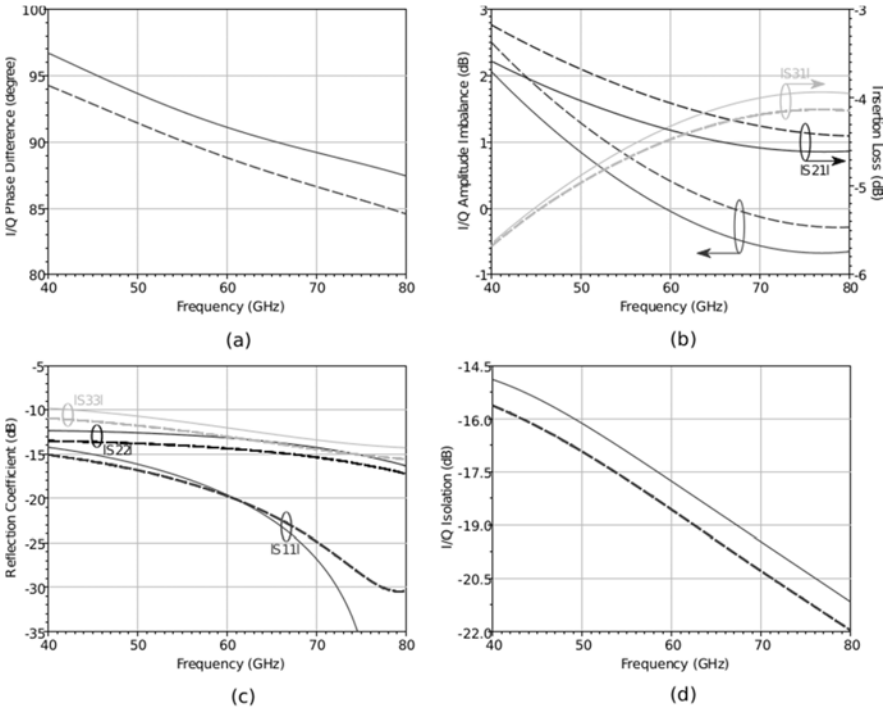

Figure 10: The performance of differential broadside coupler: (a) phase difference, (b) insertion loss, (c) reflection coefficient, (d) isolation.

In the 40 GHz bandwidth, phase imbalance of the BSC is lower than 5°, and amplitude imbalance is lower than 2 dB. Reflection coefficients at inputs and outputs are lower than -10 dB, thus an excellent matching is achieved without any additional matching structures. Impact of the mismatch and process variations of termination resistors on phase and amplitude imbalance is lower than 1.1º and 0.18 dB. Also, the load mismatch effect on the phase and amplitude imbalance is lower than 1.5º and 0.25 dB.

3.3 Poly-phase filter

Two stage PPF is designed for 60 GHz band as follows. Central operating frequency f_1 for the first stage is 62.25 GHz, and for the second stage f_2 is 59.25 GHz. Capacitance is chosen to be the same in both stages and equal to 39 fF. This is quite small value for the given technology, thus the series connection of four capacitors with capacitance of 156 fF is used. The resistance of the first stage is then $R_1 = 64.75\Omega$, and the resistance of the second stage is $R_2 = 68\Omega$. Dimensions of the designed PPF are 130 μm x 80 μm, and 3D preview is shown in Figure 11.

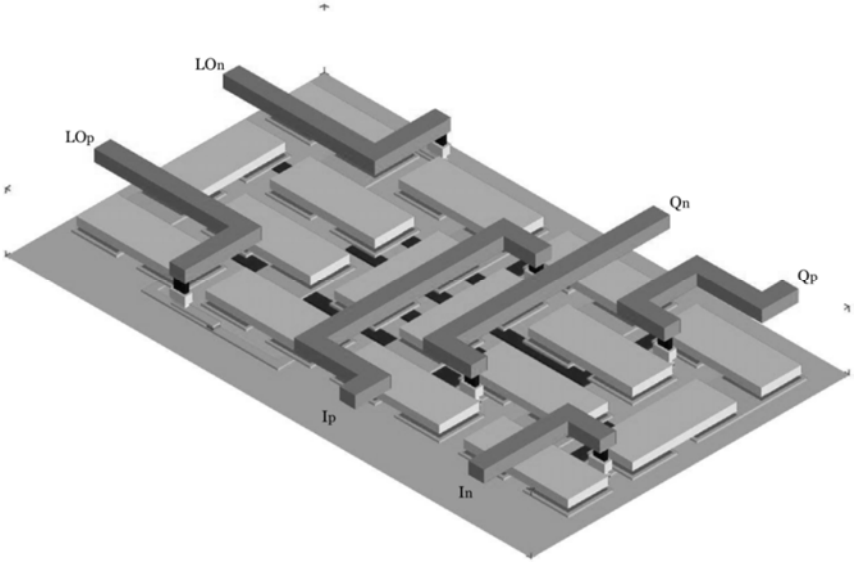

Figure 11: 3D preview of the 60 GHz poly-phase filter.

The performance of the 60 GHz PPF are shown in Figure 12. The phase imbalance is less than 2.5° at a 40 GHz range, but the PPF has significantly poorer matching.

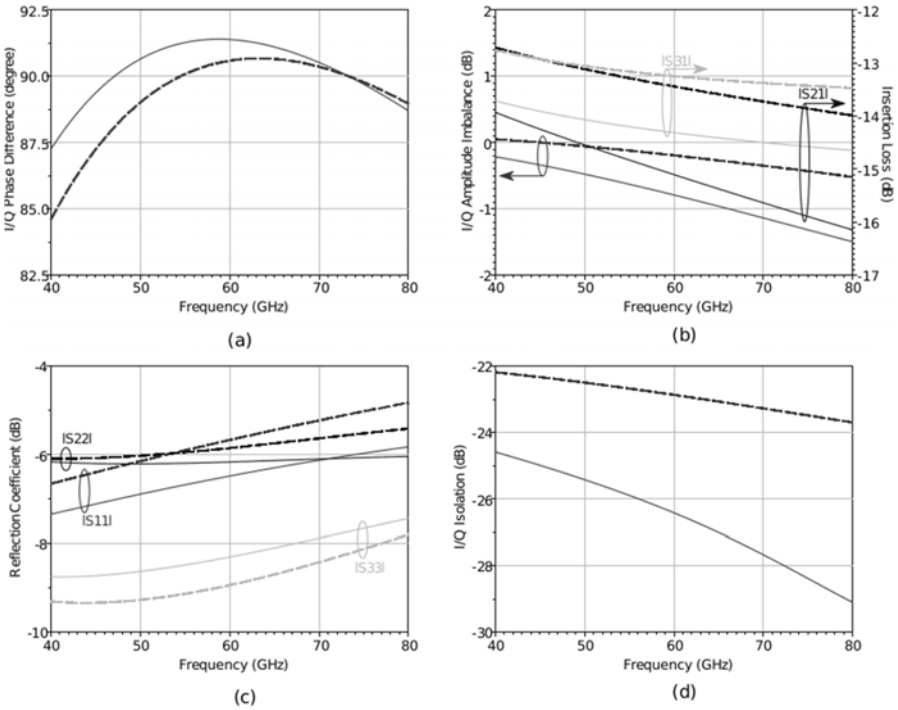

Figure 12: The performance of the 60 GHz poly-phase filter: (a) phase difference, (b) insertion loss, (c) reflection coefficient, (d) isolation.

Impact of the mismatch and process variations of resistors and MIM capacitors on the phase and amplitude imbalance is lower than 0.6º and 0.1 dB making PPF very robust to mismatch and process variations. Load mismatch effect on the phase and amplitude imbalance is lower than 3.8º and 1 dB, which shows that the PPF is very sensitivity on output load mismatch.

The performance summary is shown in Table 1.

Table 1: Overview of 60 GHz passive circuits for I/Q generation

Reference	Type	Pol.[a]	BW [GHz]	$\lvert S_{ii}\rvert$[b] [dB]	$\lvert S_{ij}\rvert$[c] [dB]	$\lvert S_{32}\rvert$ [dB]	PI [^{0}]	AI [dB]	Area [μm^2]
[1]	BLC	S.e.	7	-11	-6	-14	$\pm 3.6°$	± 0.75	370×270
[24]	Lange	S.e.	60	-16	-4.5	-14	$\pm 9.6°$	± 2.25	300×160
[24]	Lange	S.e.	60	-13	-4.5	-11	$\pm 11.5°$	± 1.75	160×120
[5]	BSC	S.e.	30	-15	-4.5	N/A	$\pm 3°$	± 0.75	280×200
[6]	BSC	Diff.	40	-13	-5	N/A	$\pm 5.3°$	± 0.6	350×175
[25]	BLC	Diff.	7	N/A	N/A	N/A	$\pm 4°$	± 0.5	400×550
[18]	PPF	Diff.	2	N/A	-10	N/A	$\pm 2.1°$	N/A	210×200
This work[d]	BLC	Diff.	7	-14	-4.5	-17	$\pm 1.7°$	± 0.4	267×230
This work[d]	BSC	Diff.	40	-10	-4.5	-15	$\pm 5°$	± 1.5	190×170
This work[d]	PPF	Diff.	40	-5	-14	-22	$\pm 2.5°$	± 0.75	130×80

[a] polarity (Pol.): single ended (S.e.) or differential (Diff.)

[b] input and output reflection coefficients: worst or any known values

[c] insertion loss: average or any known value

[d] simulation results

4 Conclusion

An overview of I/Q generation circuits for the 60 GHz band is presented in this paper. The three most suitable and most common topologies are chosen to be designed in a modern BiCMOS process.

In comparison to other I/Q generation circuits, BSC exhibits the best performance. The main advantages of this design over other references is a small area and small phase error over a 40 GHz frequency range. Insertion loss is comparable to theoretical values, thus it does not require an additional amplification stage. In a 7 GHz bandwidth around 60 GHz it presents supreme performance. All of these parameters highlight BSC as the first choice for an I/Q generation block in modern CMOS designs, in millimeter-wave integrated circuits. A possible drawback of this design is the usage of a specific metal stack. Depending on the vertical spacing between metal layers used for the implementation of the coupler, desired even- and odd-mode impedances may not be achievable.

On the other hand, BLC is implemented in the same metal layer and does not have the technology related drawbacks. Small areas can be obtained using meandering and capacitive termination of $\lambda/4$ lines. However, using capacitive termination of $\lambda/4$ lines leads to increased phase and amplitude deviation related with process and mismatch variations of used capacitors. Phase error in a 7 GHz bandwidth around 60 GHz is noticeably low and all ports are well matched. Insertion loss and output isolation are equally good as for BSC. However, BLC occupies a larger area than BSC.

A poly-phase filter is used as the third I/Q generation circuit for applications in the 60 GHz band. This solution can be used in situations where area is critical. However, PPF has huge insertion losses and has large sensitivity on the output load impedance mismatch. These are the reasons why PPF requires additional output buffer amplifiers. PPF matching is also poor, and additional matching networks are mandatory. The greatest advantage of PPF is its robustness on process and mismatch variations, and a very small phase difference over a very wide frequency range.

References

1. C. Marcu, D. Chowdhury, C. Thakkar, J.D. Park, L.K.Kong, M. Tabesh, Y. Wang, B. Afshar, A. Gupta, A. Arbabian, S. Gambini, R. Zamani, E. Alon, and A.M. Niknejad, "A 90 nm CMOS Low-Power 60 GHz Transceiver With Integrated Baseband Circuitry," IEEE Journal of Solid-State Circuits, vol. 44, pp. 3434–3447, December 2009.

2. K.J. Koh, J.W. May, and G.M. Rebeiz, "A Millimeter- Wave (40-45 GHz) 16-Element Phased-Array Transmitter in 0.18-μm SiGe BiCMOS Technology," IEEE Journal of Solid-State Circuits, vol. 44, pp. 1498–1509, May 2009.

3. M. Tabesh, J. Chen, C. Marcu, L. Kong, S. Kang, A.M. Niknejad, and E. Alon, "A 65 nm CMOS 4-Element Sub-34 mW/Element 60 GHz Phased-Array Transceiver," IEEE Journal of Solid-State Circuits, vol. 46, pp. 3018– 3032, December 2011.

4. Y. Zhao, E. Ojefors, K. Aufinger, T.F. Meister, and U.R. Pfeiffer, "A 160-GHz Subharmonic Transmitter and Receiver Chipset in an SiGe HBT Technology," IEEE Transactions on Microwave Theory and Techniques, vol. 60, pp. 3286–3299, October 2012.10

5. I. Nasr, H. Knapp, K. Aufinger, R. Weigel, and D. Kissinger, "A 50-100-GHz Highly Integrated Octave-Bandwidth Transmitter and Receiver Chipset in 0.35-μm SiGe Technology," IEEE Transactions on Microwave Theory and Techniques, vol. 62, pp. 2118–2131, September 2014.

6. M. Abbasi, S. Carpenter, H. Zirath, and F. Dielacher, "A 80-95 GHz direct quadrature modulator in SiGe technology," in 2014 IEEE 14th Topical Meeting on Silicon Monolithic Integrated Circuits in Rf Systems (SiRF), Newport Beach, 2014, pp. 56–58, IEEE.

7. W.L. Chan and J.R. Long, "A 56-65 GHz Injection-Locked Frequency Tripler With Quadrature Outputs in 90-nm CMOS," IEEE Journal of Solid-State Circuits, vol. 43, pp. 2739–2746, December 2008.

8. M.D. Tsai and A. Natarajan, "60GHz passive and active RF-path phase shifters in silicon," in 2009. RFIC 2009. IEEE Radio Frequency Integrated Circuits Symposium, Boston, 2009, pp. 223–226, IEEE.

9. C. Zhou, L. Zhang, Y. Wang, Z. Yu, and H. Qian, "A 4-bit CMOS phase shifter for millimeter-wave phased arrays," Analog Integrated Circuits and Signal Processing, vol. 79, pp. 461–468, June 2014.

10. A. Vahdati, D. Parveg, M. Varonen, M. Karkkainen, D. Karaca, and K.A.I. Halonen, "W-band phase shifter in 28-nm CMOS," Analog Integrated Circuits and Signal Processing, vol. 84, pp. 399–408, September 2015.

11. K. Scheir, G. Vandersteen, Y. Rolain, and P. Wambacq, "A 57-to-66GHz quadrature PLL in 45nm digital CMOS," in 2009. ISSCC 2009. IEEE International Solid-State Circuits Conference - Digest of Technical Papers, San Francisco, 2009, pp. 494–495, IEEE.

12. X. Yi, C.C. Boon, H. Liu, J.F. Lin, and W.M. Lim, "A 57.9-to-68.3 GHz 24.6 mW Frequency Synthesizer With In-Phase Injection-Coupled QVCO in 65 nm CMOS Technology," IEEE Journal of Solid-State Circuits, vol. 49, pp. 347–359, February 2014.

13. U. Decanis, A. Ghilioni, E. Monaco, A. Mazzanti, and F. Svelto, “A Low-Noise Quadrature VCO Based on Magnetically Coupled Resonators and a Wideband Frequency Divider at Millimeter Waves,” IEEE Journal of Solid-State Circuits, vol. 46, pp. 2943–2955, December 2011.

14. J.F. Buckwalter, A. Babakhani, A. Komijani, and A. Hajimiri, “An Integrated Subharmonic Coupled-Oscillator Scheme for a 60-GHz Phased-Array Transmitter,” IEEE Transactions on Microwave Theory and Techniques, vol. 54, pp. 4271–4280, December 2006.

15. A. Musa, R. Murakami, T. Sato, W. Chiavipas, K. Okada, and A. Matsuzawa, “A 58-63.6GHz quadrature PLL frequency synthesizer in 65nm CMOS,” in 2010 IEEE Asian Solid State Circuits Conference (A-SSCC), Beijing, 2010, pp. 1–4, IEEE.

16. T. Hirota, A. Minakawa, and M. Muraguchi, “Reduced Size Branch-Line and Rat-Race Hybrids for Unipolar MMIC’s,” IEEE Transactions on Microwave Theory and Techniques, vol. 38, no. 3, pp. 270–275, March 1990.

17. J. Kim and J.G. Yook, “A Miniaturized 3 dB 90 ◦ Hybrid Coupler Using Coupled-Line Section With Spurious Rejection,” IEEE Microwave and Wireless Components Letters, vol. 24, no. 11, pp. 766–768, November 2014.

18. M.G.M. Notten and H. Veenstra, “60GHz Quadrature Signal Generation with a Single Phase VCO and Polyphase Filter in a 0.25µm SiGe BiCMOS technology,” in IEEE Bipolar/BiCMOS Circuits and Technology Meeting. 2008, pp. 178–181, IEEE.

19. I. Sarkas, M. Khanpour, A. Tomkins, P. Chevalier, P. Garcia, and S.P. Voinigescu, “W-band 65-nm CMOS and SiGe BiCMOS transmitter and receiver with lumped I-Q phase shifters,” in 2009. RFIC 2009. IEEE Radio Frequency Integrated Circuits Symposium, Boston, 2009, pp. 441–444, IEEE.

20. W. Shin and G.M. Rebeiz, “60 GHz active phase shifter using an optimized quadrature all-pass network in 45nm CMOS,” in 2012 IEEE MTT-S International Microwave Symposium Digest (MTT), Canada, 2012, pp. 1–3, IEEE.

21. E.J. Wilkinson, “An N-Way Hybrid Power Divider,” IRE Transactions on Microwave Theory and Techniques, vol. 8, pp. 116–118, January 1960.

22. B.M. Schiffman, “A New Class of Broad-Band Mi- crowave 90-Degree Phase Shifters,” IRE Transactions on Microwave Theory and Techniques, vol. 6, pp. 232– 237, April 1958.

23. J. Lange, “Interdigitated Strip-Line Quadrature Hybrid,” in 1969 G-MTT International Microwave Symposium. 1969, pp. 10–13, IEEE.

24. M.K. Chirala and B.A. Floyd, “Millimeter-Wave Lange and Ring-Hybrid Couplers in a Silicon Technology for E- Band Applications,” in 2006. IEEE MTT-S International Microwave Symposium Digest. 2006, pp. 1547–1550, IEEE.

25. B.A. Floyd, S.K. Reynolds, U.R. Pfeiffer, T. Zwick, T. Beukema, and B. Gaucher, “SiGe bipolar transceiver circuits operating at 60 GHz,” IEEE Journal of Solid- State Circuits, vol. 40, pp. 156–167, January 2005.